Research

Proteomic and Genomic Analyses of the Rvb1 and Rvb2 Interaction Network upon Deletion of R2TP Complex Components*[S]

Mahadevan Lakshminarasimhan‡¶, Gina Boanca‡, Charles A. S. Banks‡, Gaye L. Hattem‡, Ana E. Gabriel‡, Brad D. Groppe‡‖, Christine Smoyer‡, Kate E. Malanowski‡, Allison Peak‡, Laurence Florens‡, and Michael P. Washburn‡§**

The highly conserved yeast R2TP complex, consisting of Rvb1, Rvb2, Pih1, and Tah1, participates in diverse cellular processes ranging from assembly of protein complexes to apoptosis. Rvb1 and Rvb2 are closely related proteins belonging to the AAA+ superfamily and are essential for cell survival. Although Rvbs have been shown to be associated with various protein complexes including the Ino80 and Swr1chromatin remodeling complexes, we performed a systematic quantitative proteomic analysis of their associated proteins and identified two additional complexes that associate with Rvb1 and Rvb2: the chaperonin-containing T-complex and the 19S regulatory particle of the proteasome complex. We also analyzed Rvb1 and Rvb2 purified from yeast strains devoid of *PIH1* and *TAH1*. These analyses revealed that both Rvb1 and Rvb2 still associated with Hsp90 and were highly enriched with RNA polymerase II complex components. Our analyses also revealed that both Rvb1 and Rvb2 were recruited to the Ino80 and Swr1 chromatin remodeling complexes even in the absence of Pih1 and Tah1 proteins. Using further biochemical analysis, we showed that Rvb1 and Rvb2 directly interacted with Hsp90 as well as with the RNA polymerase II complex. RNA-Seq analysis of the deletion strains compared with the wild-type strains revealed an up-regulation of ribosome biogenesis and ribonucleoprotein complex biogenesis genes, down-regulation of response to abiotic stimulus genes, and down-regulation of response to temperature stimulus genes. A Gene Ontology analysis of the 80 proteins whose protein associations were altered in the *PIH1* or *TAH1* deletion strains found ribonucleoprotein complex proteins to be the most enriched category. This suggests an important function of the R2TP complex in ribonucleoprotein complex biogenesis at both the proteomic and genomic levels. Finally, these results demonstrate that deletion network analyses can provide novel insights into cellular systems. ***Molecular & Cellular Proteomics 15: 10.1074/mcp.M115.053165, 960–974, 2016.***

The *Saccharomyces cerevisiae* R2TP complex consists of Rvb1, Rvb2, Pih1 (protein interacting with Hsp90) and Tah1 (TPR (tetratricopeptide repeat)-containing protein associated with Hsp90) proteins. Although, the R2TP complex was initially discovered in yeast as an Hsp90-associated complex (1), R2TP subunits are conserved in higher eukaryotes and the R2TP complex was recently identified and purified from human cells (2). The R2TP complex has been implicated in various cellular processes such as assembly of small nucleolar ribonuclearprotein (snoRNP)[1] (small nucleolar ribonucleoprotein) complex (3, 4), RNAPII (RNA polymerase II) complex (5), apoptosis (6), and PIKK (phosphatidylinositol 3-kinase-related protein kinases) signaling (7). The involvement of R2TP in assembling various complexes seems to be in part because of Pih1 and Tah1, which serve as adapter/recruiter proteins. For example; the

From the ‡Stowers Institute for Medical Research, Kansas City, Missouri 64110 and §Department of Pathology & Laboratory Medicine, University of Kansas Medical Center, Kansas City, Kansas 66160

Received June 25, 2015, and in revised form, January 28, 2016
Published, MCP Papers in Press, February 1, 2016, DOI 10.1074/mcp.M115.053165

Author contributions: M.L., L.F., and M.P.W. designed research; M.L., G.B., A.E.G., B.D.G., C.S., K.E.M., and A.P. performed research; G.B., C.A.B., G.L.H., and L.F. contributed new reagents or analytic tools; M.L., G.B., C.A.B., G.L.H., B.D.G., and M.P.W. analyzed data; M.L., C.A.B., G.L.H., L.F., and M.P.W. wrote the paper.

[1] The abbreviations used are: snoRNP, small nucleolar ribonucleoprotein; AAA+, adenosine triphosphatase associated with diverse cellular activities; AP-MS, affinity purification-mass spectrometry; CAM, chloroacetamide; CCTC, chaperonin-containing T-complex; dBNSAF, distributed bait normalized spectral abundance factor; dNSAF, distributed normalized spectral abundance factor; dS, distributed spectral counts; DTT, dithiothreitol; GEO, gene expression omnibus; FDR, false discovery rate; FPKM, fragments per kilobase of exon per million fragments mapped; GO, gene ontology; HDAC1, histone deacetylase 1; IDR, intrinsically disordered regions; IFN, interferon; ISGs, IFN-α-stimulated genes; MudPIT, multidimensional protein identification technology; NCBI, national center for biotechnology information; Pih1, protein interacting with Hsp90; PIKK, phosphatidylinositol 3-kinase-related protein kinases; PLGEM, power law global error model; PMSF, phenylmethylsulfonyl fluoride; RNAPII, RNA polymerase II; RPM, revolutions per minute; Tah1, TPR repeat-containing protein associated with Hsp90; TAP, tandem affinity purification; TCA, trichloroacetic acid; TCEP, tris-(2-carboxyethyl)-phosphine hydrochloride; TEV, tobacco etch virus; TPR, tetratricopeptide repeat; YPD, yeast peptone dextrose.

cytoplasmic assembly of human RNAPII complex involves a cochaperone, the Prefoldin-like complex. Both the Prefoldin-like complex and RNAPII complex are recruited by the R2TP complex (8). Tah1 has been shown to directly interact with Rpb1 (the largest subunit of RNAPII) and possibly bring the R2TP and Prefoldin-like complexes together to facilitate RNAPII complex assembly (5). Similar examples illustrate an adaptor/recruiter function for Pih1 in recruiting the Hsp90 chaperone to other complexes. These include the recruitment of Hsp90 to the yeast box C/D snoRNP assembly via an interaction between Pih1 and Nop58 (4) and the activation of PIKK signaling by recruitment of Hsp90 to PIKK via an interaction between Pih1 and the PIKK subunit Tel2 (9).

Rvb1 and Rvb2 (Tip49 and Tip48 in humans) are members of the AAA+ (adenosine triphosphatase associated with diverse cellular activities) superfamily possessing both ATPase as well as helicase activities (10). Rvb1 and Rvb2 are similar in both sequence and structure across various species and are essential for cell survival (11). This comes as no surprise, because they are involved in several biological processes ranging from assembly of macromolecular complexes (with or without the involvement of Pih1 and Tah1), chromatin remodeling and the regulation of gene transcription (12, 13). Rvb1 and/or Rvb2 have also been linked to human diseases and are overexpressed in lung, liver, and colon cancers (12). Both Rvb1 and Rvb2 form higher order oligomers either by themselves or together, which can influence their activity, function and association with other protein complexes (14–17). Electron microscopy studies on Swr1 indicate that Rvb1 and Rvb2 exist as heterohexamer (16, 18), whereas instances of both single heterohexameric and dodecameric ring structures have been observed in the Ino80 complex (15, 18). The oligomerization of Rvb1/Rvb2 in several complexes is an intense field of study, and it is becoming widely accepted that the molecular organization of these proteins are complex and species dependent. Based on structural studies, Rvb1 and Rvb2 have been divided into three domains. The N and C terminus of Rvbs form part of the AAA+ domain (domain I and II respectively, which includes the classical Walker A and B motifs, Sensors and Arginine finger) and the enigmatic insertion region (domain II) which is ~174 amino acids long and protrudes from the ring like oligomeric structures formed by Rvbs (19). The insertion region has been proposed to play roles in the activity of Rvb1/2, nucleic acid binding and in protein-protein interactions.

Pih1 (originally known as Nop17 and referred to as Pih1D1 in humans) is a ~40 KDa protein which is unstable on its own, but is stable when bound to Tah1 (20). Pih1 is predominantly localized in the nucleolus. Pih1 contains a Pih1 domain at its N terminus, two IDRs (intrinsically disordered regions) and a C-terminal region, which is highly susceptible to degradation. Using bioinformatics analysis and mutational studies, Paci *et al.* (20) have shown that the IDR1 of Pih1 is largely responsible for Rvb1/Rvb2 binding, and the IDR2 and C terminus are needed for binding to Tah1. Tah1 (RPAP3 or hSpagh in humans) is the smallest member of the complex with 111 amino acids and connects Pih1 to Hsp90. Tah1 contains 2 TPR (tetratricopeptide repeat) motifs which are responsible for binding to the C terminus (MEEVD motif) of Hsp90 and the unfolded C-terminal segment (93–111) of Tah1 is responsible for binding to and stabilizing Pih1 (21).

Despite recent advances in characterizing the Rvb1, Rvb2, and the R2TP complex, there is no comprehensive information available on associations between the members of this complex and other cellular proteins. Here, we have used a combination of AP-MS (affinity purification-mass spectrometry) based proteomic analysis and deletion network analysis to create a protein association network centered on Rvb1/Rvb2. We show that yeast Rvb1 and Rvb2 together associate with several protein complexes, which we ranked based on quantitative proteomic data. AP-MS analyses using yeast strains lacking *PIH1* and *TAH1* indicate that Rvb1/Rvb2 associate independently with both Hsp90 and the RNAPII complex. In support of this independent association, *in vitro* binding studies suggest direct interactions between Rvb1/Rvb2 and Hsp90 or between Rvb1/2 and the RNAPII complex. Intriguingly, we noticed an enhanced interaction between Rvb1/Rvb2 and Hsp90/RNAPII complex in the absence of Pih1. RNA-Seq analysis of these deletion strains yielded unexpected links to gene expression changes in ribosome biogenesis, ribonucleoprotein complex biogenesis, abiotic stimulus, and response to temperature stimulus. Finally, a GO analysis of the 80 proteins found altered in protein associations in all four deletion strains found ribonucleoprotein complex proteins to be the most enriched category suggesting an important function of the R2TP complex in this process.

EXPERIMENTAL PROCEDURES

Cloning and Expression of Recombinant Proteins from Insect Cells—Rvb1, Rvb2 and Hsp90 from *Saccharomyces cerevisiae* were amplified using custom designed primers (supplemental Table S1) and cloned in pBACPAK8™ vector (Clontech Laboratories, Mountain View, CA) for recombinant expression in a Baculovirus system. Rvb1 contained TEV (tobacco etch virus) protease cleavable 6xHis tag, Rvb2 contained FLAG tag and Hsp90 contained TEV protease cleavable Halo tag (Promega, Madison, WI) at their respective N termini. Tags for Rvb1 and Rvb2 were introduced by incorporating the corresponding sequences in primers, whereas TEV cleavable Halo-tag was first introduced into pBACPAK8™ vector before cloning the Hsp90 gene. pBACPAK8™ vectors containing the genes of interest were used to generate baculoviruses using the BacPAK™ expression system (Clontech Laboratories). 500 ml of ~1 million Sf21 cells/ml cultured at 27 °C in Sf-900III SFM media (Life Technologies, Grand Island, NY) were infected with baculoviruses containing individual His-Rvb1, FLAG-Rvb2 and Halo-Hsp90 (separately or together). Infected cells were harvested after 48 h and stored at −80 °C until required.

Purification of Recombinant Proteins from Insect Cells—Sf21 cells expressing His-Rvb1 were resuspended in 25 ml of lysis buffer (50 mM Tris, pH 7.5, 300 mM NaCl, 10 mM imidazole) containing protease inhibitors (0.1 mM benzamidine HCl, 55 μM phenanthroline, 10 μM bestatin, 20 μM leupeptin, 5 μM pepstatin A and 1 mM PMSF (phen-

ylmethylsulfonyl fluoride) and passed five times through an 18-gauge needle for lysis. Lysed cells were centrifuged at 19,000 RPM (revolutions per minute) for 40 min in Beckman Coulter Avanti J20-XPi centrifuge using a Ti25.50 rotor (Beckman Coulter, Brea, CA). Clarified lysates were mixed with Ni-NTA Agarose resin (Qiagen, Valencia, CA) that was equilibrated with lysis buffer and incubated for 1 h at 4 °C followed by collection of the flow-through. The resin was washed with 10 bed volumes of wash buffer (lysis buffer containing imidazole at a final concentration of 20 mM). The protein was eluted by adding lysis buffer containing imidazole at a final concentration of 200 mM. Flag tagged Rvb2 was purified similarly to Rvb1 using ANTI-FLAG® M2 affinity gel (Sigma-Aldrich, St. Louis, MO) but with different buffers. Lysis buffer for Rvb2 purification contained: 50 mM Tris, pH 7.5, 150 mM NaCl and protease inhibitors. Wash buffer contained 50 mM Tris, pH 7.5, 300 mM NaCl and protease inhibitors. The protein was eluted by incubating the resin with 150 ng/μl 3× FLAG peptide (Sigma-Aldrich) for 1 h at 4 °C. Halo tagged Hsp90 was also purified similarly to Rvb1 but using 1× PBS (phosphate buffered saline) (10 mM phosphate buffer, pH 7.4, 2.7 mM KCl, 137 mM NaCl). Hsp90 was eluted by incubating Hsp90 bound HaloLink™ Sepharose resin (Promega) with His tagged AcTEV™ protease (Life Technologies) for 1 h at 4 °C in TEV cleavage buffer. The eluted proteins were dialyzed overnight in 25 mM HEPES, pH 7.5, 50 mM KCl, 1 mM DTT (dithiothreitol) buffer. Dialyzed Hsp90 was passed through Ni-NTA resin and the flow-through was collected to remove the AcTEV protease. The proteins were further purified by anion exchange chromatography (1 ml HiTrap DEAE Sepharose FF resin (GE Healthcare Bio-Sciences)) using the AKTA protein purification system (GE Healthcare Bio-Sciences).

Cloning, Expression and Purification of Proteins from Saccharomyces cerevisiae—All *Saccharomyces cerevisiae* (yeast) BY4741 strains used in this study were obtained from GE Healthcare Dharmacon Research's yeast collection (formerly Open Biosystems). TAP (tandem affinity purification) tags were introduced at the 3′ end of Rvb1 and Rvb2 (in *PIH1* and *TAH1* deletion strains) by homologous recombination using an amplicon that contained a selection marker (S.D.-URA) and gene sequence corresponding to the TAP tag (custom designed primers, supplemental Table S1). TAP tagged wild-type Rvb1, Rvb2 and Rpb1 strains were purchased from GE Healthcare. Cells were grown in YPD (yeast peptone dextrose) media to an OD_{600} of 1.25–1.50 and protein purification was performed as described previously (22). RNAPII complex was prepared by first performing a TAP tag purification using TAP tagged Rpb1 (similarly to Rvb1 and Rvb2) followed by anion exchange chromatography (1 ml HiTrap DEAE Sepharose FF resin (GE Healthcare Bio-Sciences)) using the AKTA protein purification system (GE Healthcare Bio-Sciences). The buffers used were 25 mM HEPES, pH 7.5, 50 mM KCl, 0.5 mM DTT, 10% (v/v) glycerol (buffer A) and 25 mM HEPES, pH 7.5, 500 mM KCl, 0.5 mM DTT, 10% (v/v) glycerol (buffer B).

Analyses of RNA Levels—Total RNA was isolated from ~5 ml yeast cells grown to an OD_{600} ~1.2 - 1.5 using the MasterPure™ yeast RNA purification kit (Epicenter, Madison, WI) followed by enrichment of poly(A)+ RNA by oligo(dT) selection which was then used to construct individually barcoded libraries with the TruSeq RNA Sample preparation kit (Illumina, San Diego, CA). All measurements were performed in triplicate. One replicate of Rvb1-TAP was discarded from further analysis after it was discovered that the sample had been mislabeled (data not shown). Sequenced libraries were aligned to the UCSC sacCer3 reference genome with Tophat (23). Read counts for each of the 7126 gene transcripts (6692 coding genes, 413 non coding genes, and 21 pseudogenes) were generated with the Rsubread package in R (24). FPKM (fragments per kilobase of exon per million fragments mapped) values were calculated in R using the DESeq2 library (25). All data files have been deposited at the GEO (gene expression omnibus) repository and can be accessed using the accession number: GSE69220.

Rvb1-TAP and Rvb2-TAP samples were compared with Rvb1/2-TAP purified Pih1Δ and Tah1Δ deletion strains using DESeq2 (25). DESeq2 models read counts as a negative binomial distribution and fits a generalized linear model for each gene. Genes were considered differentially expressed if they had a p value<0.01 and a log2 fold change>0.7. An additional filtering step removed lowly expressed genes with an average FPKM<10. To visualize the differences between the top genes from each comparison we clustered the regularized log2 transformed data from DESeq2 using the default hierarchical clustering method in R with a Euclidean distance measure. The resulting data is displayed as a heatmap created with the R package pheatmap (Raivo Kolde (2015). pheatmap: Pretty Heatmaps. R package version 1.0.2. http://CRAN.R-project.org/package=pheatmap). The data is shown with standard row scaling to highlight the differences of individual genes across samples. To perform qPCR, total RNA was reverse transcribed using iScript™ Reverse Transcription Supermix (Bio-Rad, Hercules, CA) and analyzed using the MyiQ™ real-time PCR detection system (Bio-Rad). The primers used for qPCR are listed in supplemental Table S1.

Mass Spectrometry Analyses—TAP tag purified proteins were precipitated overnight with 25% (v/v) TCA (trichloroacetic acid) and washed twice with ice cold acetone, air dried, resuspended in 100 mM Tris-HCl, pH 8.5, 8 M Urea, followed by incubation with 5 mM TCEP (tris-(2-carboxyethyl)-phosphine hydrochloride) then with 10 mM CAM (chloroacetamide) to reduce and alkylate disulfide bonds respectively. 0.5 μg of Sequencing grade Endoprotease Lys-C (Roche, Indianapolis, IN) was added to the samples and incubated at 37 °C for 6 h, diluted with 100 mM Tris, pH 8.5 to reduce the concentration of Urea to 2 M, supplemented with 2 mM $CaCl_2$ and further incubated with 0.5 μg sequencing grade Trypsin (Promega) (overnight) and quenched with 5% (v/v) formic acid (J.T.Baker, Center Valley, PA). Tryptic digests were loaded on to tri-phasic 100 μm fused silica microcapillary columns that were placed in-line with an HPLC (Agilent, Santa Clara, CA) coupled LTQ mass spectrometer (Thermo Scientific, Waltham, MA) and 12, ~2 h MudPIT steps were performed as described in Florens *et al.* (26). Database matching and data analyses were performed as described in Banks *et al.* (27). Briefly, the .raw files from the MS runs were processed by in-house generated RAWDistiller v. 1.0 software (28) to generate .ms2 files from which the MS/MS spectra were matched to a database using SEQUEST algorithm (Version 27, rev.9) (29). Mass tolerance for precursor ion was set at 3 Da and fragment ion tolerance was set to the default value of 0 in the sequest.params file. To account for carboxamidomethylation, a static modification of +57 Da was added to cysteine residues. To account for oxidation of methionine residues, variable search was carried out with +16 Da. No enzyme specificity was imposed during searches. The database used for the search was from NCBI (national center for biotechnology information, release date April 26, 2011) and contained a total of 11,990 sequences, out of which 5819 belonged to non-redundant *Saccharomyces cerevisiae* proteins. The rest of the sequences comprised of 176 commonly found contaminants (such as IgGs, human keratin and proteolytic enzymes) and shuffled sequences of *Saccharomyces cerevisiae* proteins and contaminants to estimate false discovery rates. The spectral FDR (false discovery rate) and protein FDR are 0.32 ± 0.16% and 4.39 ± 1.98% respectively (from 5 controls and 18 experimental samples of yeast TAP purifications) (supplemental Table S2). The database used for searching proteins that were produced in insect cells were from release date April 24, 2011 and contained a total of 150,494 sequences out of which 58,776 belonged to non-redundant proteins. The rest of the sequences comprised of 181 commonly found contaminants (such as IgGs, human keratin and proteolytic enzymes). The spectral FDR was

0.13±.09% and protein FDR was 4.60 ± 4.70% (from four samples that were searched using the insect cell database) (supplemental Table S2). DTASelect/Contrast (30) was used for filtering the peptides/spectra using the following criteria: minimum DeltCn = 0.08; minimum XCorr values of 1.8, 2.0 and 3.0 for singly, doubly and triply charged spectra respectively; Sp rank of 10.0 and a minimum peptide length of 7 amino acids. Only fully tryptic peptides were considered for analyses. The proteins that were subsets of others were removed using the parsimony option. If proteins were identified by the same set of peptides (including at least one peptide unique to the set to distinguish between isoforms), they were grouped together; one representative accession number was used to describe the set. A total of 23 MudPIT runs were performed in this study. All the .RAW, .ms2 and .sqt files have been uploaded in the MassIVE database and can be found using the following ids: MSV000079137 and MSV000079332 (ftp://MSV000079137@massive.ucsd.edu & ftp://MSV000079332@massive.ucsd.edu) and password: r2Tp_1. Four wild-type runs were used from the Sardiu *et al.* study (31).

RESULTS

MudPIT Analyses of TAP Tagged Rvb1 and Rvb2 Identify New Complex Associations—To determine the proteins associated with Rvb1 and Rvb2, yeast strains containing a TAP tag at the C-terminal end of either Rvb1 or Rvb2 (referred to as wild-type strains or bait proteins) were cultured and the bait proteins were purified using the TAP tag purification protocol (22). Because the TAP tag was integrated into the yeast genome, endogenous protein expression levels were maintained and spurious associations caused by of protein overexpression were avoided. Three independent purifications for experimental samples (tagged) and five purifications for control (untagged) were subjected to MudPIT analyses. Each sample was split into 3 equal parts and subjected to individual MudPIT runs to account for technical variations (technical replicates). After MudPIT analyses, separate SEQUEST (29) searches were performed on each replicate followed by DTASelect (30). Another round of DTASelect was performed to merge all the technical replicates and subjected to Contrast (30) and NSAF7 software (32) analyses to compare and contrast the different runs. For quantitative comparison, we used the label free spectral counting approach as described in Zhang *et al.* (32), where distributed spectral counts (based on unique and shared spectra) were used for label-free quantitation. MudPIT analyses of TAP tag purified Rvb1 and Rvb2 from wild-type and *PIH1* and *TAH1* deletion strains show that Tah1 is present only in the presence of Pih1, whereas Pih1 is pulled-down even in the absence of Tah1 (Fig. 1*A*). Because our method captures complexes that are assembled *in vivo*, it confirms that Pih1 bridges Rvb1/Rvb2 and Tah1, and is indispensable for the formation of the R2TP complex as has been discussed previously (4).

Using the PLGEM (power law global error model) algorithm (33), we identified a set of proteins (prey) specifically enriched in the wild-type Rvb1 and/or Rvb2 bait purifications, but not in the untagged control purifications. To avoid false positives such as contaminants and nonspecific proteins, only proteins appearing in at least two out of three purifications (>50%) were taken into consideration for PLGEM analysis. PLGEM uses dNSAF values to estimate the likelihood of proteins being enriched in experimental samples over controls and calculates *p* values for each prey which are further used to determine FDR using the Benjamini and Hochberg method (34). Only proteins with an FDR of 5% or less were used in further analyses, thus ensuring a stringent selection process. Of the 414 Rvb1 associated proteins and 299 Rvb2 associated proteins that were identified, 236 copurified with both Rvb1 and Rvb2 (Fig. 1*B* and supplemental Tables S3, S4). Among the 236 proteins that passed our criteria, 28 proteins are already known to be associated with or interact with both Rvb1 and Rvb2. Examples include proteins from the R2TP, Ino80, Swr1 and ASTRA complexes (Fig. 1*C* and supplemental Table S5).

We found several protein complexes which had not been previously reported as associating with the Rvb proteins. In particular, we identified a relatively large number of spectra corresponding to subunits of both the CCT (chaperonin-containing T-complex) complex and the proteasome. The CCT complex (GO (gene ontology) id: 0005832) mediates protein folding and the proteasome complex (GO id: 0000502) is involved in protein degradation. Specifically, we were able to capture all 11 proteins belonging to the CCT complex (albeit some with lower spectral counts) and several subunits of the 26S proteasome complex (Fig. 1*D*, Fig. 1*E* and supplemental Tables S3–S5). To corroborate our approach, we also analyzed the wild-type data against an unrelated TAP tagged control (Rtt101) (supplemental Tables S3, S4) and found that neither the CCT nor proteasome were enriched in the Rtt101 pull-downs whereas contaminating proteins were generally at the same abundances, ruling out nonspecific interactions via the TAP tag. It is interesting to observe that Rvbs have been found to be associated with both protein folding and protein degradation machinery in the cells and thus expanding the network of proteins associated with Rvbs.

Label free quantitative proteomics provides a deeper understanding of the Rvb1 and Rvb2 associated proteins than the qualitative data available in databases like the Saccharomyces Genome Database (SGD) (www.yeastgenome.org), for example (35). In SGD, Rvb1 is listed to have 102 physical interactions, and 82 genetic interactions with 9 identified by both physical and genetic methods. While this is important prior knowledge, these lists provide no ranking of interactions, which quantitative proteomic methods can provide. The top associated proteins of Rvb1-TAP are shown in Fig. 2*A* sorted from highest to lowest abundance. When summing the abundances of proteins that are only found in specific complexes, the largest abundance originates from Ino80 at 21% followed by Swr1 at 10%, the proteins specific to the R2TP complex at 4%, and then the proteasome at 3% (Fig. 2*A*). In SGD Rvb2 is listed to have 131 physical interactions and 87 genetic interactions with seven identified by both physical and genetic methods. The top associated proteins of Rvb2-TAP are

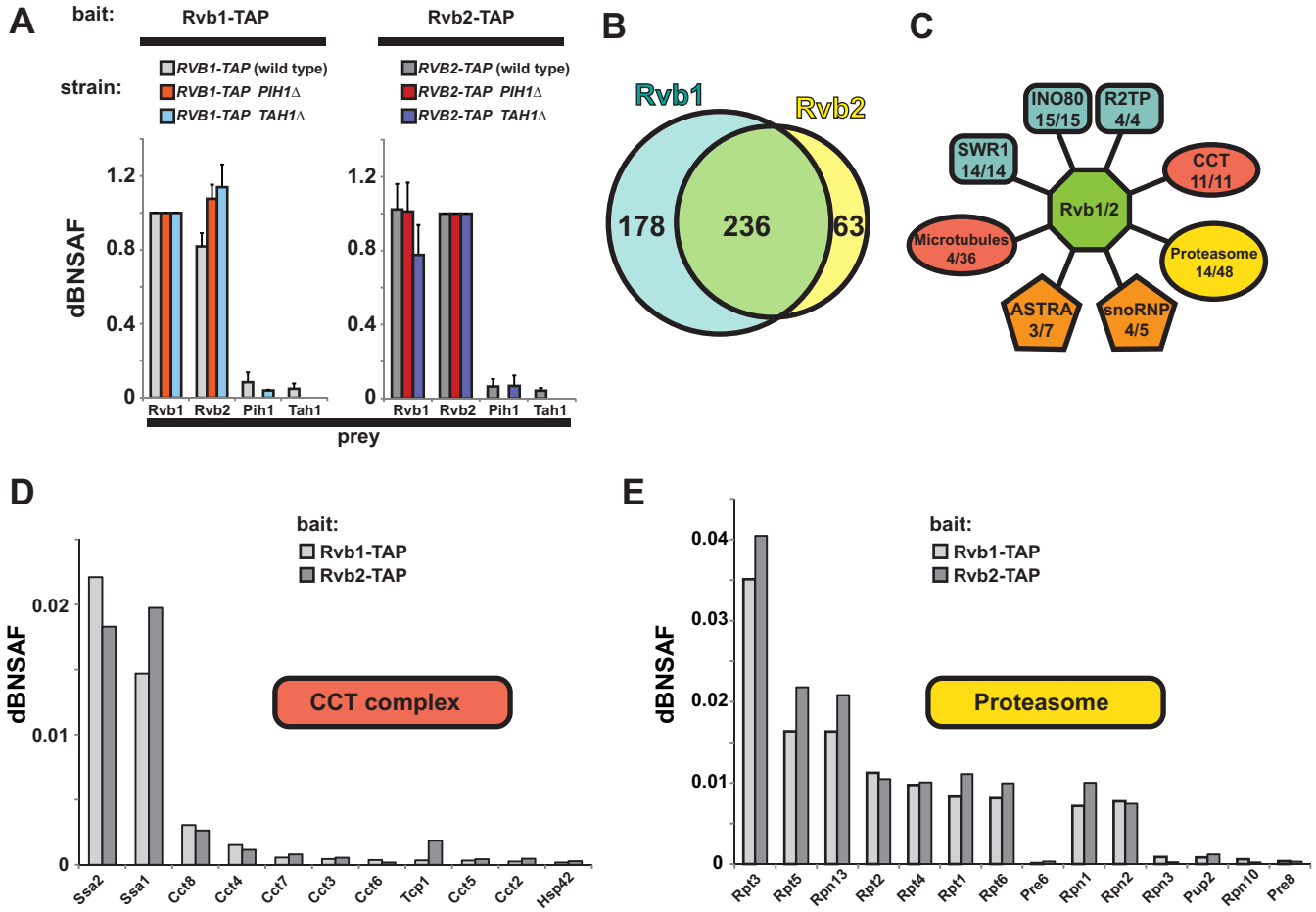

FIG. 1. **Rvb1 and Rvb2 both associate with the other R2TP subunits Pih1 and Tah1, and copurify with a functionally diverse group of other protein complexes.** *A*, components of the R2TP complex copurify with Rvb1 and Rvb2. Either Rvb1-TAP or Rvb2-TAP associated proteins were isolated from whole cell extracts of the strains indicated by TAP purification, and identified using MudPIT mass spectrometry. Relative amounts of each protein are estimated using dBNSAF values, where the dNSAF value for each protein was divided by the dNSAF value of the bait protein. The average relative amounts of the four R2TP subunits Rvb1, Rvb2, Pih1, and Tah1 are indicated (average dBNSAF values calculated from 3 biological replicates). Error bars indicate standard deviation. *B*, Rvb1/Rvb2 associated proteins. Proteins enriched in the Rvb1 and Rvb2 purified wild-type samples described in *A*, but not in control purifications were identified by PLGEM analysis as previously described (22) (FDR <0.05, except for: the snoRNP subunit Nop56; the CCT complex components Cct2, Cct6, Hsp42, Ssa1 and Ssa2). The area proportional Venn diagram was generated using "Venn Diagram Plotter" (PNNL, http://omics.pnl.gov/). *C*, protein complexes captured by Rvb1/2. For each complex the number of complex components captured (left) and the total number of known subunits for each complex (right) is indicated. *D* and *E*, dBNSAF values of CCT and proteasome complex components that are present in both Rvb1 and Rvb2 purifications.

shown in Fig. 2*B* sorted from highest to lowest abundance. When summing the abundances of proteins that are only found in specific complexes, the largest abundance originates from Ino80 at 33% followed by Swr1 at 6%, the proteasome at 4%, and then the proteins specific to the R2TP complex at 3% (Fig. 2*B*).

The mass spectrometry based estimated copies per cell (CpC) of these proteins from Kulak *et al.* (36) is shown in Fig. 2*C*. No value of Tah1 is available in this data set and Act1 at 117,202 CpC was excluded from the graph for visualization purposes. The proteasome components identified in this study are overall about six times more abundant than Ino80 components and 15 times more abundant than Swr1 components based on CpC estimates from Kulak *et al.* (36). When comparing the CpC estimates in Fig. 2*C* to the ranked abundances in Figs. 2*A* and 2*B*, the increased association of Rvb1 and Rvb2 with Ino80 when compared with Swr1 is likely explained by the larger amount of Ino80 in the cell. Given the much higher abundance of the proteasome and the lower levels of the proteasome associated with Rvb1-TAP and Rvb2-TAP when compared with Ino80 and Swr1, it is likely that Rvb1-TAP and Rvb2-TAP are only associating with a small subpopulation of the proteasome.

Rvb1 and Rvb2 Interact Directly With Hsp90—Having defined a set of Rvb1 and Rvb2 associated proteins; we noticed that Hsc82 (yeast systematic name: YPL240C and hereafter called Hsp90 for convenience) was present in both wild-type and mutant purifications (Fig 3*A*). This raises the possibility

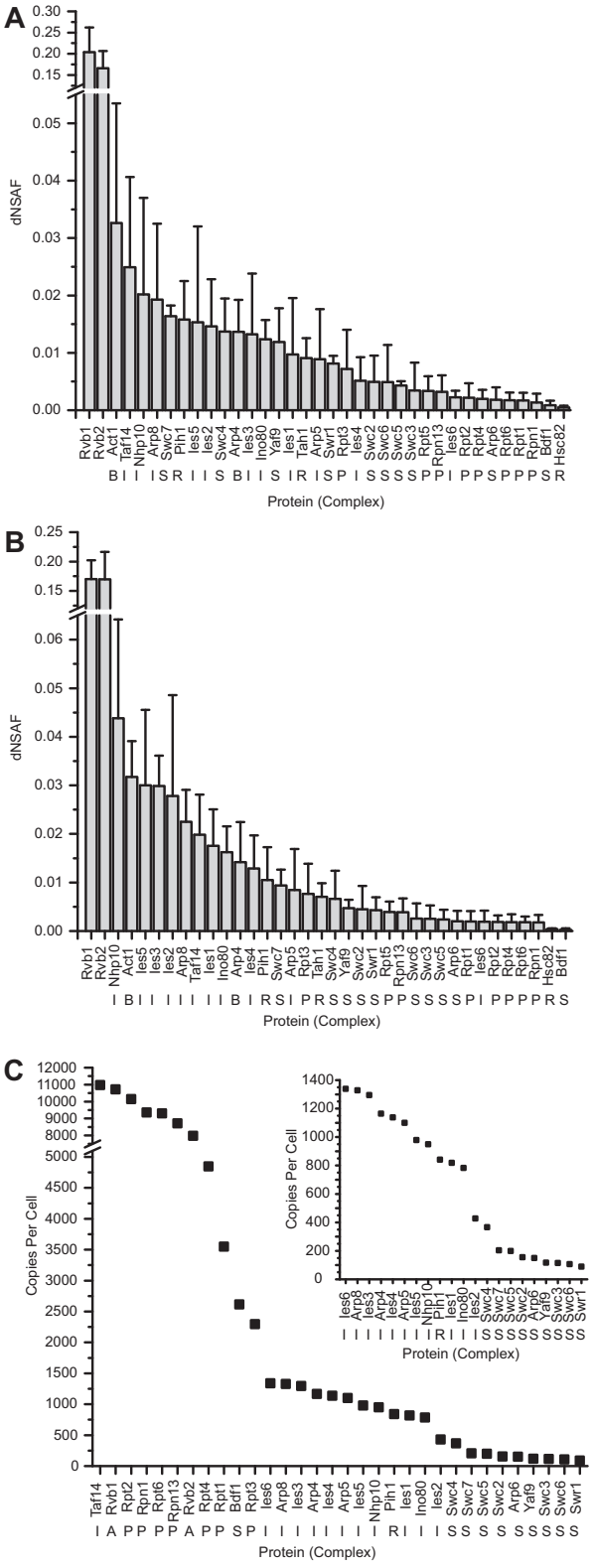

FIG. 2. **Quantitative Proteomic Analysis of Top Rvb1/2 Interacting Proteins.** *A*, Thirty six of the top proteins interacting with Rvb1 sorted from highest to lowest abundance after contaminant extraction. The focus of the graph is on proteins from the Ino80 complex (I), Swr1 complex (S), the Proteasome (P), the R2TP complex (R), and proteins in both Ino80 and Swr1 (*B*). The first 33 proteins are the 33 most abundant proteins found in the Rvb1-TAP purification after contaminant extraction. The average and standard deviation is shown for three biological replicates. *B*, Thirty six of the top proteins interacting with Rvb2 sorted from highest to lowest abundance after contaminant extraction. The focus of the graph is on proteins from the Ino80 complex (I), Swr1 complex (S), the Proteasome (P), the R2TP complex (R), and proteins in both Ino80 and Swr1 (*B*). The first 34 proteins are the 34 most abundant proteins found in the Rvb2-TAP purification after contaminant extraction. The average and standard deviation is shown for three biological replicates. *C*, The Copies per Cell information (36) was available for 35 of the 36 proteins listed in *A* and *B* (Tah1 missing from CpC data, while Act1, Hsc82 and Rpt5 were excluded for scale purpose). The inset graph is an expansion of the Ino80 (I) and Swr1 (S) specific components demonstrating the higher abundance of Ino80 proteins *versus* Swr1 proteins.

that Hsp90 either directly interacts or associates with Rvb1 and/or Rvb2. To further analyze this finding, we cloned Rvb1, Rvb2, and Hsp90 in to pBACPAK8™ vectors with different tags as mentioned in the experimental section. When Sf21 cells were co-infected with viruses containing 6xHis tagged Rvb1, Flag tagged Rvb2 and Halo tagged Hsp90 and proteins were purified using the Flag resin, we observed 2 predominant bands in Coomassie stained gels, which corresponding to Hsp90 and Rvb1/2 (Fig. 3*B*, lane F). Western blot analysis of the Flag elution (lane F) confirmed that the upper band corresponds to Halo tagged Hsp90 (~116 kDa) and the other predominant band (~53 kDa) contains both 6xHis-TEV-Rvb1 (~52.9 kDa) and FLAG-Rvb2 (~53 kDa) (Fig. 3*B*, right panel). In order to test if the co-elution of Hsp90 with Rvb1/2 is because of direct interaction, elution fractions from the FLAG purification were further purified using Ni-NTA chromatography, which enriches for His tagged proteins. Analysis of fractions from the His tag purification by MudPIT mass spectrometry (Fig. 3*B* lane K) confirmed the presence of Rvb1, Rvb2 and Hsp90 (Fig. 3*B*), indicating a robust interaction between Hsp90 and Rvb1/2.

To dissect the nature of interactions between the individual subunits, we performed a second series of experiments in which we first purified the Rvb1, Rvb2 and Hsp90 proteins individually, and then mixed the purified proteins together in various combinations to test for protein–protein interactions using affinity chromatography (Fig. 3*C*). Hsp90 copurified with His-Rvb1 (Fig. 3*C second panel*), FLAG-Rvb2 (Fig. 3*C third panel*) as well as in the presence of both Rvb1 and Rvb2 (Fig. 3*C* end of *third panel*). It is unlikely that other proteins mediate this interaction as we did not detect significant amounts of other proteins in the eluate when we analyzed it by MudPIT (Fig. 3*C fourth panel*). To rule out any possibility of nonspecific interactions between Rvb1/2 and Hsp90, we performed the same experiment using yeast alcohol dehydrogenase (Sigma-Aldrich, catalogue no. A7011). No interactions were observed between alcohol dehydrogenase and either of the Rvbs (supplemental Fig. S1), indicating specific and genuine interaction between Rvbs and Hsp90.

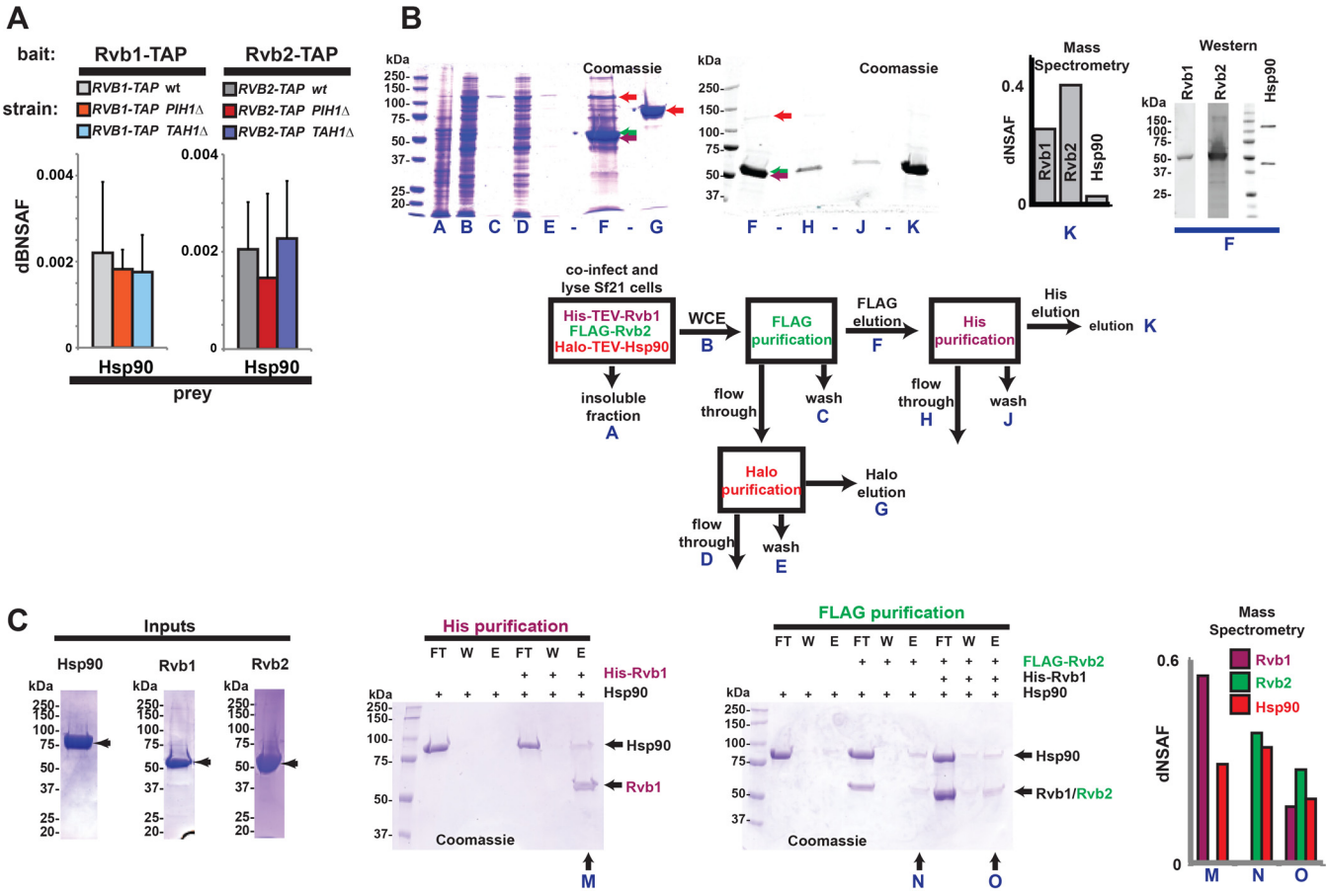

FIG. 3. **Rvb1 and Rvb2 interact directly with Hsp90.** *A*, Hsp90 copurifies with Rvb1/2 complexes purified from *S. cerevisiae*. Average dBNSAF values for Hsp90 are from the 3 biological replicates; error bars are standard deviation. *B*, recombinant Hsp90 expressed in Sf21 cells interacts with recombinant Rvb1/2 in the absence of other yeast proteins. Sf21 cells coinfected with baculoviruses encoding His-TEV-Rvb1, FLAG-Rvb2 and Halo-TEV-Hsp90 were prepared as described in Experimental Procedures. Affinity purifications were performed as shown in the purification scheme and various fractions were analyzed by SDS-PAGE and proteins visualized by staining with Coomassie Blue R-250. In addition, Western blot (on fraction F) and mass spectrometry (fraction K) analyses were performed to test for the presence of Rvb1, Rvb2 and Hsp90. Please note because one gel had high background, we scanned the Coomassie stained gel as a black and white image using the Odyssey Infrared Imaging system (LI-COR, Lincoln, NE), which improves the resolution of the gel. *C*, interaction between purified recombinant Hsp90 mixed with either purified Rvb1 or Rvb2. Sf21 cells were infected with baculoviruses encoding affinity tagged Rvb1, Rvb2 or Hsp90 and these proteins were affinity purified individually. Samples containing ~50 μg of each protein were mixed and incubated for 30 min at room temperature in the combinations indicated. Mixtures were subjected to either His (Ni-NTA) purification or FLAG purification, the indicated fractions analyzed by SDS-PAGE, and proteins visualized by staining with Coomassie Blue R-250. Elution fractions from all 3 purifications (fractions M, N and O) were subjected to mass spectrometry analysis to confirm the presence of proteins of interest. Abbreviations: FT = flow through; W = wash; E = elution. Color coded arrows represent proteins presented in the purification scheme.

Altered Rvb1/2 Associations in the Absence of Pih1 and Tah1—Having identified a set of Rvb1/2 associated proteins, we investigated whether Pih1 and Tah1 might have a role in regulating which proteins associate with Rvb1/2. To this end, MudPIT analyses of TAP tag purifications from Pih1 and Tah1 deletion strains were further analyzed using PLGEM statistics (as described above) to identify proteins enriched with Rvb1/2 specifically in these mutant strains. While performing PLGEM statistics, proteins which appeared > 50% of the time in the mutant purification and were at least twofold enriched compared with wild-type were considered for further analyses. We used enrichment cut-off instead of FDR, since PLGEM is less reliable when working with smaller datasets. The number of proteins that passed our criteria were 511 (*RVB1-TAP PIH1*Δ), 585 (*RVB1-TAP TAH1*Δ), 286 (*RVB2-TAP PIH1*Δ), and 730 (*RVB2-TAP TAH1*Δ), of which 80 were present in all mutant purifications. (Fig. 4*A* and supplemental Table S6). Among these 80 proteins, 16 were exclusively present in the mutant strain purifications (Fig. 4*B*, Table 1) and GO analysis of these proteins revealed that the majority of them are not part of any complex. However, the GO Slim Mapper function in SGD revealed that the top two most represented GO terms of these 80 proteins was ribonucleoprotein complex and periribosome (supplemental Table S6). Among the proteins that were still present in wild-type purifications albeit in lower proportions, both the RNAPII complex (Rpb1 and Rbp2) and the snoRNP

A

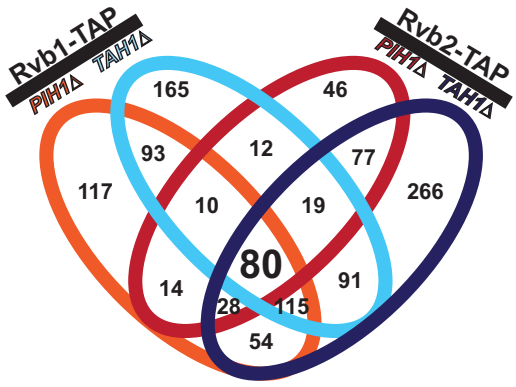

B

Table 1:

Prey	GO term ID	GO term name	distributed spectra					
			Bait: Rvb1-TAP			Bait: Rvb2-TAP		
			wt	*PIH1*Δ	*TAH1*Δ	wt	*PIH1*Δ	*TAH1*Δ
Mgm101p	~	~	0.0	29.3	16.0	0.0	10.0	4.3
Krr1p	30529	ribonucleoprotein complex	0.0	6.7	3.0	0.0	1.3	5.0
Cdc28p	30529	ribonucleoprotein complex	0.0	1.8	4.3	0.0	4.9	4.8
YPL150W	~	~	0.0	3.3	2.3	0.0	1.3	7.0
Ppz1p	~	~	0.0	8.7	2.3	0.0	3.0	0.7
Pmd1p	~	~	0.0	10.3	5.3	0.0	3.7	2.7
Lcb5p	~	~	0.0	7.7	3.3	0.0	4.0	4.7
YDR333C	~	~	0.0	6.0	7.0	0.0	2.7	9.7
Xdj1p	~	~	0.0	3.0	3.7	0.0	0.7	3.7
Fab1p	70772	PAS complex	0.0	7.0	4.3	0.0	1.0	2.3
Elp3p	33588	elongator holoenzyme complex	0.0	6.0	6.0	0.0	2.7	16.3
Apm1p	30120	vesicle coat	0.0	5.0	3.3	0.0	3.0	9.0
Mfb1p	151	ubiquitin ligase complex	0.0	1.0	3.7	0.0	1.3	3.3
Atg1p	34273	ATG1/UKL1 signaling complex	0.0	4.7	2.3	0.0	1.7	5.0
Srp40p	~	~	0.0	2.0	1.0	0.0	1.0	2.0
Zds2p	~	~	0.0	2.3	1.3	0.0	1.3	1.3

Table 2:

Prey	distributed spectra									
	Bait: Rvb1-TAP					Bait: Rvb2-TAP				
	wt	*PIH1*Δ	*PIH1*Δ / wt	*TAH1*Δ	*TAH1*Δ / wt	wt	Pih1Δ	Pih1Δ / wt	Tah1Δ	Tah1Δ / wt
Rpb1	38.7	1221.0	31.6	115.0	3.0	6.3	33.7	5.3	86.0	13.6
Rpb2	21.3	324.0	15.2	82.3	3.9	5.3	36.0	6.8	66.3	12.4
Nop1	4.0	105.3	26.3	76.7	19.2	41.3	145.0	3.5	103.0	2.5
Nop56	24.9	199.5	8.0	150.8	6.1	37.7	112.5	3.0	136.8	3.6

FIG. 4. **R2TP complexes lacking subunits Pih1 or Tah1 have an increased association with components of the RNA polymerase II and snoRNP complexes.** *A*, a subset of proteins associate with Rvb1 and Rvb2 complexes purified without Pih1 or Tah1. Proteins present in the indicated purifications (described in Fig. 1), but not in control purifications, were identified using PLGEM analysis. The Venn diagram was generated using "Venny" (*Oliveros, J.C. (2007–2015) Venny. An interactive tool for comparing lists with Venn's diagrams.* http://bioinfogp.cnb.csic.es/tools/venny/). *B*, increased association of a set of proteins with Rvb1/2 in the absence of Pih1 or Tah1. Table I, representative proteins from the common 80 proteins shown in *A*, which are enriched in purifications using *PIH1*Δ or *TAH1*Δ deletion strains, compared with purifications using the wild-type strains. Average distributed spectral counts (dS) from three biological replicates are shown. Table II, RNAPII and snoRNP subunits are enriched in Rvb1/2 -TAP purifications using strains lacking the *PIH1* or *TAH1* genes (RNAPII subunits- Rpb1 and Rpb2: snoRNP subunits- Nop1 and Nop56).

assembly complex (Nop1 and Nop56) were enriched with Rvb1/2 in much greater amounts in the absence of Pih1 and/or Tah1 (Fig. 4*B*, Table 2). In particular, the largest subunits of the RNAPII complex, Rpb1 (also known as Rpo21) and Rpb2, copurified with Rvb1 in more than 10 fold greater amounts in the absence of Pih1 (Fig. 4*B*, Table II).

Rvbs Interact Directly With the RNA Polymerase II Complex—Rvb1/2 appears to strongly associate with RNAPII complex subunit Rpb1 in the absence of Pih1; this could be the result of direct physical interactions between the two. To address this, we first wanted to validate the association between the Rvbs and RNAPII complex in yeast. Elution fractions from purified TAP tagged Rvb1 and Rvb2 were subjected to Western blot analysis using Rpb1 antibody (Fig. 5*A*). The amounts of Rvb1 or Rvb2 in the purified samples are similar for all strains used (detected using an antibody specific to C terminus of the TAP tag). In contrast, Rpb1 is enriched in purifications performed from mutant strains, particularly in *RVB1-TAP PIH1*Δ and *RVB2-TAP TAH1*Δ strains (Fig. 5*A*, left panel, Fig. 5*B* and supplemental Fig. S2). Western blot analysis shows no difference in expression levels of Rpb1 protein when comparing the *RVB2-TAP PIH1*Δ and *RVB2-TAP TAH1*Δ to the wild-type strain. However, MudPIT analyses demonstrated that Rpb1 in indeed enriched in *RVB2-TAP PIH1*Δ and *RVB2-TAP TAH1*Δ strains (Fig. 5*B* right panel). This is likely due to the differences in sensitivity between Western blotting, which is dependent on antibody sensitivity, and quantitative proteomics.

To rule out that the Rpb1 enrichment seen is not simply due to Rpb1 protein overexpression in the deletion strains, we analyzed Rpb1 levels in the whole cell extracts and quantified them relative to tubulin (Fig. 5*A* right panel). Rpb1 protein is detected at approximately the same levels in all strains. In

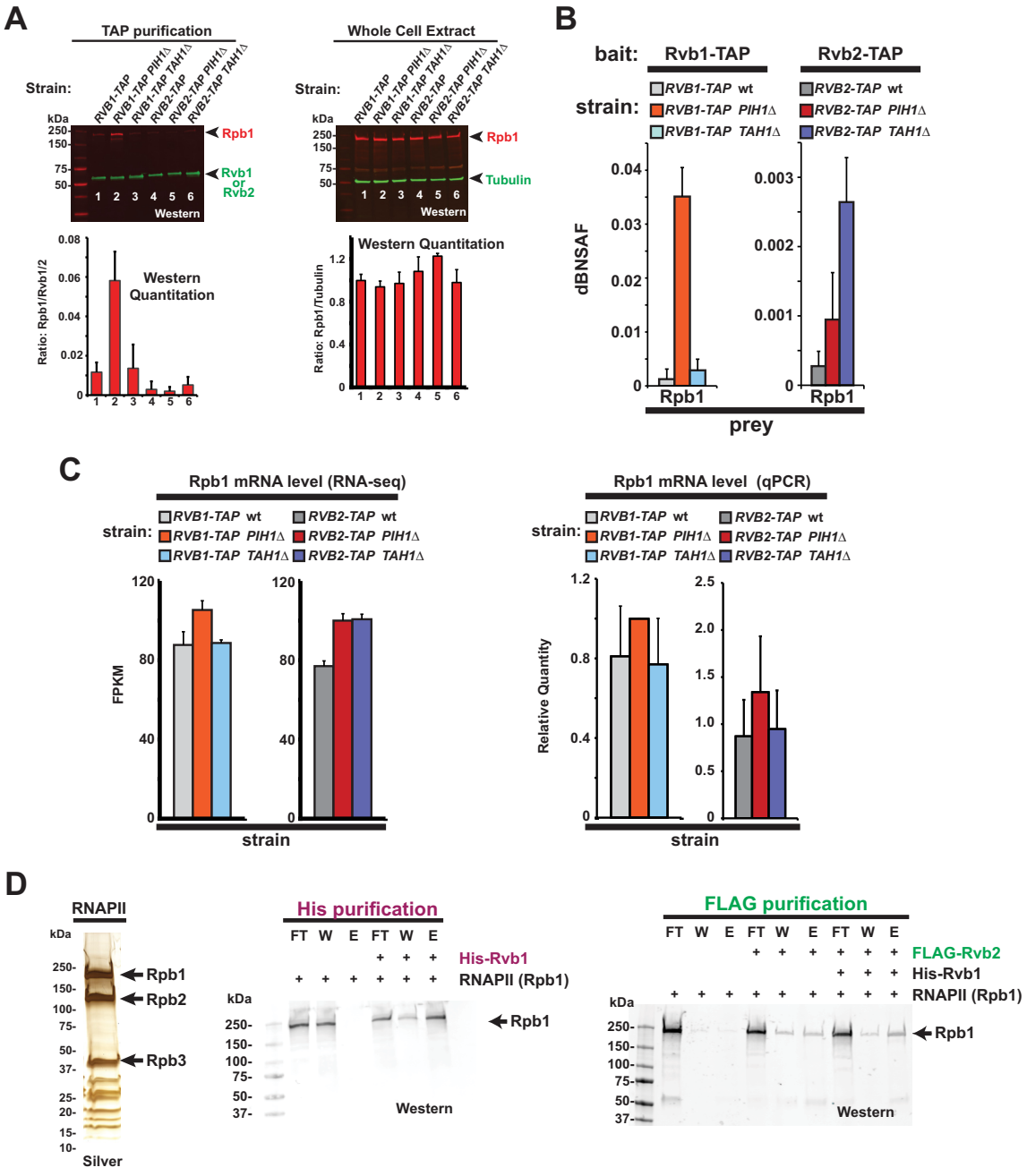

FIG. 5. **Interaction between Rvb1/2 and RNApolymerase II complex.** *A*, *left* panel, TAP-purified samples of the indicated strains were analyzed by Western blotting. Rvb1/2 proteins were visualized with rabbit anti-TAP polyclonal antibodies and IRDye®800CW anti-rabbit secondary antibodies (green). Rvb1 associated proteins purified from *S. cerevisiae* lacking Pih1 are enriched for the pol II subunit Rpb1. *A*, *right* panel, Whole cell extracts prepared from the indicated yeast strains were analyzed for the presence of RNAPII subunit Rpb1 by fractionating samples using SDS-PAGE and detecting proteins by Western blotting. Rpb1 was detected with mouse anti-Rpb1 monoclonal antibodies and IRDye® 680LT anti-mouse secondary antibodies (red); tubulin was detected with rabbit anti-tubulin monoclonal antibodies and IRDye®800CW anti-rabbit secondary antibodies (green). Li-Cor Odyssey software was used for both imaging and band quantitation. Band quantitation was repeated on Western blots for three biological replicates; average values are plotted. *B*, Rpb1 association with Rvb1 or Rvb2 depends on Pih1 and Tih1. Average dBNSAF values were calculated from the purifications used in Fig. 1. *C*, the absence of Pih1 or Tah1 does not significantly affect Rpb1 mRNA levels. RNA samples purified from whole cell extracts of the indicated strains were analyzed by either RNA-seq or qPCR as described in Experimental Procedures. *D*, interaction between RNA polymerase II purified from yeast and either recombinant Rvb1 or Rvb2 isolated from Sf21 insect cells. Representative Silver stained gel showing purified RNAPII complex that was used as input (for inputs of Rvb1 and Rvb2 refer to Fig. 2*C* left panel). Approximately 10 μg samples of Rvb1, Rvb2 or RNAPII complex were mixed in the combinations indicated, affinity purified, and analyzed by SDS-PAGE and Western blotting.

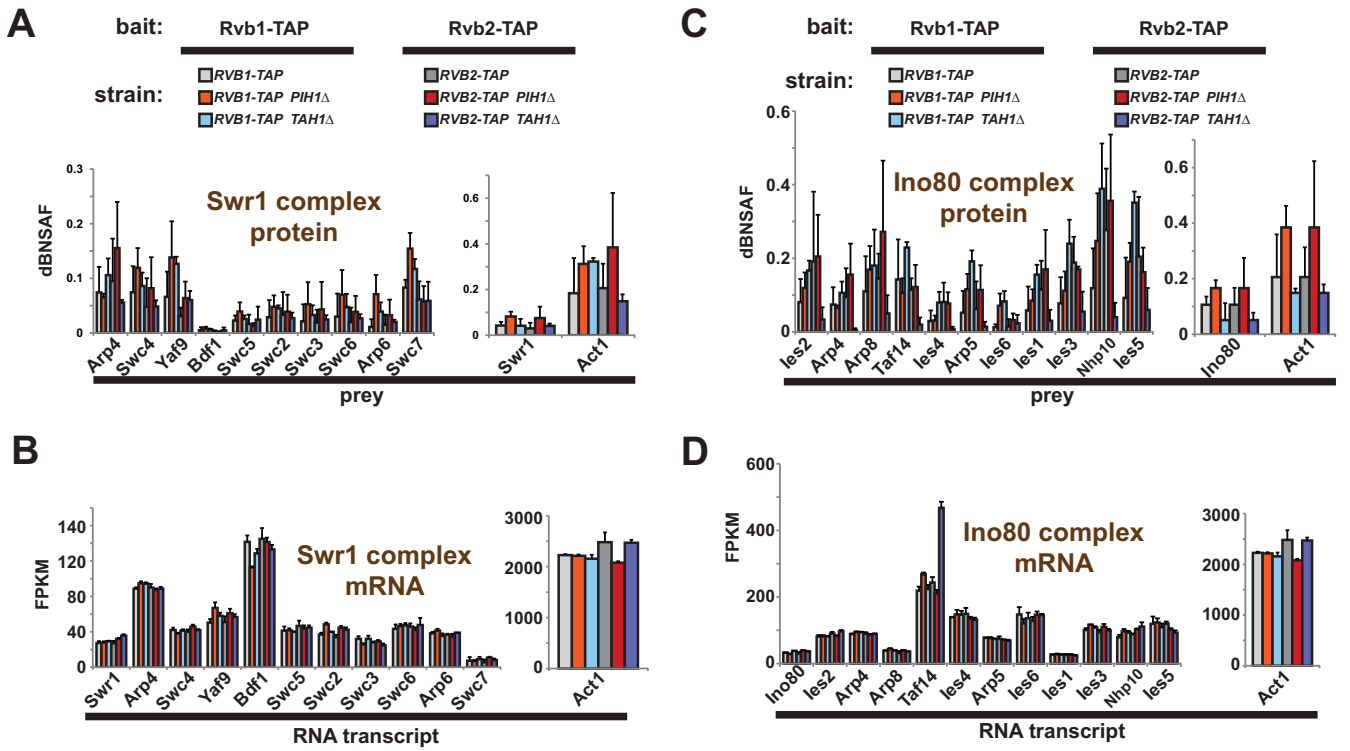

FIG. 6. **Association between R2TP (with or without Pih1 or Tah1), and the Swr1 and Ino80 complexes.** *A, B*, association of Swr1 complex subunits with R2TP with or without Pih1 or Tah1. *A*, components of the Swr1 complex were identified in the samples described in Fig. 1*A*. 1*B*, the relative amounts of the mRNA transcripts corresponding to each Swr1 subunit were calculated by using RNA-seq to analyze samples of total RNA purified from whole cell extracts. FPKM = *f*ragments *p*er *k*ilobase (of exon) per *m*illion (fragments mapped). *C, D*, association of Ino80 complex subunits with R2TP with or without Pih1 or Tah1.

addition, we analyzed Rpb1 transcript levels using both RNA-seq. and quantitative PCR (Fig. 5*C*), and again observed small significant differences between the wild-type and mutant strains that are likely not biologically relevant and do not reach the magnitude of protein changes. To further investigate the nature of interaction between the RNAPII complex and Rvb1/2, we performed *in vitro* pull down experiments using recombinant yeast Rvb1 and Rvb2 and the RNAPII complex. Purified Rvb1, Rvb2 and RNAPII complex were mixed in different combinations as shown in Fig. 5*D* and subjected to either Ni-NTA (His) or FLAG affinity chromatography. The RNAPII complex (identified by the detection of Rpb1 in the elution fractions) copurifies with Rvb1, with Rvb2, and with both proteins together (Fig. 5*D*). This is consistent with direct interactions between surfaces on RNAPII and both Rvb1 and Rvb2. We were also able to detect all of the RNAPII subunits in elution fractions (Fig. 5*D* right panel last lane) using MudPIT analysis (data not shown), indicating that Rvbs might interact with intact RNAPII complexes.

Recruitment of Rvb Proteins to the Chromatin Remodelers Swr-C and Ino80-C—It is well known that Rvbs are essential for cell survival and are part of several protein complexes, but it is unclear how they are recruited to these complexes. After investigating the Pih1 and Tah1 dependent recruitment of Rvb1/2 to RNAPII, we analyzed our proteomics data set to try to determine whether Pih1 and Tah1 are involved in recruitment of the Rvbs to the Ino80 and Swr1 chromatin remodeling complexes. To address this, we analyzed the MudPIT data from wild-type and mutant Rvb1/2-TAP strains to determine the relative amounts of Swr1 or Ino80 subunits copurifying with Rvb1/2 in the presence or absence of Pih1 or Tah1 (Fig. 6*A* and 6*C*). In addition, we monitored the transcript levels of Ino80 and Swr1 complex subunits in each strain to exclude the possibility that any effects that we observed resulted from changes in Swr1 or Ino80 gene expression (Fig. 6*B* and 6*D*). We found that deleting the *PIH1* or *TAH1* genes did not result in an overall decrease in the amount of Ino80 and Swr1 complex components copurifying with Rvb1 or Rvb2; indicating that the incorporation of Rvbs into these complexes does not depend on either Pih1 or Tah1. This is in contrast to the findings of Zhao *et al.* (1), who report that in the absence of Pih1 and Tah1, Rvb1 and Rvb2 are enriched in Ies2-TAP purifications, a key component of the Ino80 complex. Nevertheless, analysis of transcript levels indicated that the only change observed was the up-regulation of *TAF14* from the *RVB2-TAP TAH1*Δ strain, which is part of Ino80 as well as several other protein complexes (37).

Analysis of RNA-Seq Data—Finally, we analyzed the RNA-Seq data to determine the global effects of deleting *PIH1* or

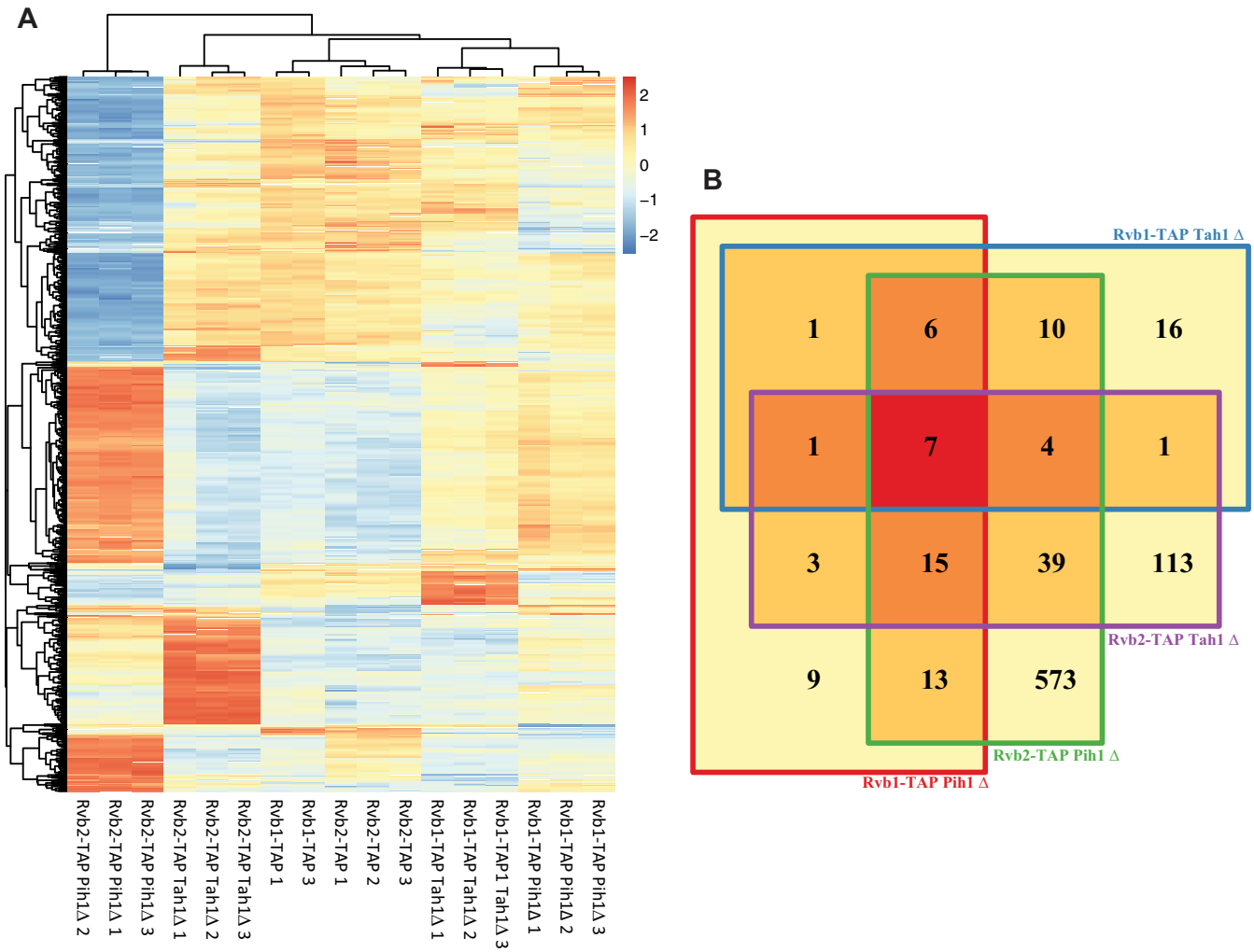

FIG. 7. **Comparison of Gene Expression Changes between Strains.** *A*, *RVB1-TAP* and *RVB2-TAP* strains were compared with *RVB1-TAP* and *RVB2-TAP* strains with *PIH1* and *TAH1* deleted. Differentially expressed genes were identified using the DESeq2 package in R (25). Genes were considered differentially expressed if they had a p value$<$0.01 and a log2 fold change$>$0.7. An additional filtering removed lowly expressed genes with an average FPKM$<$10. The top genes were clustered with the default hierarchical clustering method in R (Raivo Kolde (2015). pheatmap: Pretty Heatmaps. R package version 1.0.2. http://CRAN.R-project.org/package = pheatmap) with a Euclidean distance measure. The heatmap created with the package pheatmap displays the data with standard row scaling to highlight the differences of individual genes across samples. *B*, The overlap of the top genes from each comparison are shown in the Venn diagram created with the Vennerable package in R (Jonathan Swinton (2013)). Vennerable: Venn and Euler area-proportional diagrams. R package version 3.0/r82. http://R-Forge.R-project.org/projects/vennerable/).

TAH1 from the *RVB1-TAP* or *RVB2-TAP* strains. All Pearson correlations were 0.994 or more (supplemental Fig. S3). These high correlation values reflect similar levels of gene expression for the majority of genes in all strains analyzed. In addition, the lower correlation values obtained when we compared some deletion strains with wild-type strains is also consistent with a limited number of gene expression changes. To assess these, we next performed a hierarchical clustering analysis of the complete dataset (Fig. 7*A*). After clustering, the replicates grouped together. Interestingly, the deletion of *PIH1* or *TAH1* had different effects depending on whether they were in the *RVB1-TAP* or *RVB2-TAP* background. To assess whether these different effects were consistent with previously reported phenotypic data, we compared annotations for mutant phenotypes of all the components of this system listed in the Saccharomyces Genome Database (35). *RVB1* has 5 phenotypes, *RVB2* has 19 phenotypes, *TAH1* has 13 phenotypes, and *PIH1* has 29 phenotypes. The shared phenotype function in SGD reports none of these phenotypes are shared between any of the components *RVB1, RVB2, PIH1,* and *TAH1*. The different effects that we observed when deleting either *PIH1* or *TAH1* in the different backgrounds (*RVB1-TAP* or *RVB2-TAP*) are consistent with previously reported data that disruptions introduced to any of these four components can have a different set of phenotypic effects.

Next, we compared the deletion strains to their respective wild-type strains to determine changes in gene expression.

We used an adjusted *p* value of less than 0.01 as the cutoff for all comparisons. A total of 55 genes had significant expression changes in the *RVB1-TAP PIH1* Δ strain with 43 downregulated and 12 up-regulated when compared with the control *RVB1-TAP* (supplemental Table S7). Next, 46 genes had significant expression changes in the *Rvb1-TAP TAH1*Δ strain with 21 downregulated and 25 up-regulated when compared with the control *RVB1-TAP* (supplemental Table S7). In the case of the *RVB2-TAP* strains, deletion of *PIH1* resulted in 667 statistically significant gene expression changes with 356 downregulated and 311 up-regulated and deletion of *TAH1* resulted in 183 statistically significant gene expression changes with 46 downregulated and 137 up-regulated. A Venn diagram analysis of the gene expression changes found in all studies is shown in Fig. 7*B*. Only seven gene expression changes were found in common in all analyses. The *PIH1* and *TAH1* deletion strains in *Rvb1-TAP* background shared 13 genes whose expression was significantly different (Fig. 7*B*). The two *TAH1*Δ strains shared 13 genes whose expression was significantly different (Fig. 7*B*). The two *PIH1*Δ strains shared 41 genes whose expression was significantly different (Fig. 7*B*).

We next conducted GO term analysis of these results (supplemental Fig. S4 and supplemental Table S8). In the *RVB1-TAP PIH1*Δ strain, ribosome biogenesis ($p = 0.022$) was up-regulated, whereas transition metal ion transport ($p = 6.55E-05$) and nucleotide biosynthetic process ($p = 2.57E-04$) were among the larger number of downregulated GO categories. In the *RVB1-TAP TAH1*Δ strain, carboxylic acid biosynthetic process ($p = 3.71E-08$), arginine biosynthetic process ($p = 7.80E-08$), and translation elongation (1.05E-04) were up-regulated, whereas response to temperature stimulus (p 4.07E-07) and transition metal ion transport ($p = 0.018874$) were among the downregulated GO categories. In the *RVB2-TAP PIH1*Δ strain, ribosome biogenesis ($p = 2.34E-98$), maturation of SSU-rRNA ($p = 2.13E-36$), RNA modification ($p = 1.66E-34$) including snoRNA 3′ end processing ($p = 0.020299$), and RNA 5′end processing ($p = 5.24E-20$) were among the many GO categories up-regulated, while response to temperature stimulus ($p = 4.09E-37$), vacuolar protein catabolic process ($p = 1.09E-31$), and protein refolding ($p = 6.68E-09$) were among the many GO categories downregulated. In the *RVB2-TAP TAH1*Δ strain, ncRNA processing ($p = 1.98E-06$), ribosome biogenesis ($p = 5.14E-05$), and RNA modification ($p = 2.29E-04$) were among the up-regulated GO categories, while polyphosphate metabolic process ($p = 4.49E-05$) and response to temperature stimulus ($p = 0.0088$) were the most enriched downregulated categories. There were common themes among these GO analyses (supplemental Fig. S4 and supplemental Table S8). Ribosome biogenesis and ribonucleoprotein complex biogenesis were up-regulated in the *RVB1-TAP PIH1*Δ strain, the *RVB2-TAP PIH1*Δ strain, and the *RVB2-TAP TAH1*Δ (supplemental Fig. S4*A*). The *RVB1-TAP TAH1*Δ strain, *RVB2-TAP PIH1*Δ strain, and the *RVB2-TAP TAH1*Δ had downregulated response to abiotic stimulus (supplemental Fig. S4*B*), and all four strains had downregulated response to temperature stimulus (supplemental Fig. S4*B*).

DISCUSSION

The highly sensitive and reproducible nature of affinity purification mass spectrometry combined with label free quantitative proteomics has played a major role in identification and characterization of new protein associations and interactions (27, 38–40). Although the yeast R2TP complex and its components have been studied before (41, 42), a comprehensive deletion network analysis is still needed. In the present study, we have purified Rvb1 and Rvb2 from wild-type yeast strains and were able to confirm the known protein associations of the Rvbs. Employing stringent selection criteria, we identified new complexes that associate with Rvb1 and Rvb2 and thus expand their association network. In particular, we observe a strong association between Rvb1 and Rvb2 to the 19S regulatory proteasome complex. All the base subunits of the 19S regulatory subcomplex were captured, including the regulatory particle of non-ATPase subunits (Rpn1, Rpn2, Rpn10, and Rpn13) and the regulatory particle of triple AAA-ATPase (Rpt1–6) subunits (43). The strong association between Rvbs and the base subunits of the 19S subcomplex is very intriguing, because the six AAA-ATPase subunits also form heterohexamers as has been observed in Rvbs and it remains to be seen if the Rvbs have any role in the assembly and oligomerization of Rtp1–6. In fact, the biogenesis of the 19S subcomplex and its association with the 20S core particle is largely uncharacterized. Hsp90 has been shown to play a role in this assembly (44), but the exact mechanism is still poorly understood. It would be interesting to determine if Rvbs play a role in recruiting Hsp90 to the 19S proteasome complex or even help in its assembly without the involvement of Hsp90. Further investigation of the association between the Rvbs and the 19S proteasome may shed more light on the assembly of the proteasome complex.

Although several proteins associated with both Rvb1 and Rvb2 baits from wild-type strains (236), considerably more proteins copurified with Rvb1 (414) than with Rvb2 (299) (Fig. 1*B*). This difference can be attributed to the instances where both proteins can act independently and even exhibit antagonistic effects (45–48). For example, in prostate cancer cells the metastasis suppressor gene KAI1 which inhibits metastasis by promoting cell adhesion, is activated by the Rvb1/Tip60 complex whereas the Rvb2/β-catenin complex along with HDAC1 (histone deacetylase 1) acts as co-repressor of the transcription of KAI1. Thus, the expression of KAI1 and its metastatic potential is regulated by the antagonistic actions for Rvb1 and Rvb2 (48). It is also worth mentioning that Rvb1 and Rvb2 cannot complement each other and have opposite polarities (Rvb1 displaces DNA from 3′ to 5′ direction (49), whereas Rvb2 displaces from 5′ to 3′ (50)), which may lead to differences in their association with other proteins.

The proteomic analyses of Rvb1 and Rvb2 purifications from *PIH1* and *TAH1* deletion strains provide interesting new information. First, purification of Rvb1 and Rvb2 in the *PIH1* and *TAH1* deletion backgrounds still retains Hsp90. It is highly unlikely that this interaction is mediated by Hsp90 cofactors, because we do not see Hsp90 cofactors associate with Rvb1/2 in stoichiometrically relevant numbers (supplemental Table S9). Further analysis of the interaction between Rvbs and Hsp90 using a biochemical approach revealed that Hsp90 directly interacts with Rvbs. To our knowledge, this is the first time a direct interaction between Rvbs and Hsp90 is being reported. Based on our findings it is clear that in yeast, Rvb1 and Rvb2 can either interact with Hsp90 as part of the R2TP complex or by themselves. Because Hsp90 can interact with Rvbs and can also aid in folding and assembly of several protein complexes, it offers a possible explanation as to why Rvb1 and Rvb2 may possess chaperone-like activity. Further characterization of the interaction between Rvb1/2 and Hsp90, such as the regions required for their interaction and the stoichiometry of the complex would offer clues about their function. Second, our analyses also revealed several interesting proteins that copurified with Rvbs only in the absence of Pih1 or Tah1 (Fig. 4*B*, Table I). One such interesting protein is Mgm101 (systematic name: YJR144W), which appears in high numbers only in the deletion strain purifications. Mgm101 is a Rad52-type mitochondrial protein that binds to single stranded DNA and has been suggested to play a role in interstrand cross-link repair of mitochondrial DNA (51). Mgm101 also oligomerizes to form rings similar to Rvbs. The bacterial RuvB helicase, which is related to Rvb1 and Rvb2 forms a double hexamer and mediates migration of Holliday junctions in double-strand break repair (52). It has been suggested that Rvbs may also play a role in double strand DNA break repair by assisting Ino80 and Swr1 complexes (53). Taken together, it is possible that Rvbs may also play a similar role in mitochondrial genome maintenance by associating with Mgm101. Finally, we observed an increase of RNAPII complex components in deletion purifications. On further investigation we were able to biochemically confirm that Rvb1/2 interacts with the RNAPII complex. Previous studies have shown that the R2TP complex is involved in the assembly of the RNAPII complex in the cytoplasm, mediated by the interaction between human hSpag1 protein (yeast Tah1 equivalent) and the Rpb1 subunit of RNAPII complex (5). Our findings indicate that yeast Rvb1/2 can interact with RNAPII even in the absence of Pih1 and Tah1, offering clues for the observation of human Ruvb1 in RNAPII complex purifications (11, 54). Rvb1 has also been shown to have a direct role in transcription initiation of ISGs (IFN (interferon)-α-stimulated genes) by recruiting RNAPII complex to its promoter region (55), but it is not known whether Rvb1 is part of yet another unidentified complex that recruits Rvb1 and RNAPII to the transcription start site. From our data it is tempting to speculate that Rvb1 may directly recruit RNAPII complex to the promoter region of ISGs.

In this study we also carried out a systematic RNA-Seq analysis of the TAP tagged strains compared with *PIH1*Δ and *TAH1*Δ deletion strains. There were common themes among the gene expression changes like changes in ribosome related GO categories (supplemental Table S8). A comparison of the changed proteins from the quantitative proteomic analysis of the *PIH1* and *TAH1* deletion strains to the RNA-Seq analysis of the same strains yields an interesting link. GO Slim Mapper analysis of 80 proteins found changed in all deletion strains (Fig. 4*A*) found ribonucleoprotein complex and periribosome to be the most enriched categories. In the RNA-Seq studies, the ribonucleoprotein complex biogenesis GO category was found enriched in the up-regulated genes in the *RVB2-TAP TAH1*Δ strain, the *RVB2-TAP PIH1*Δ strain, and the *RVB1-TAP PIH1*Δ strain (supplemental Fig. S4). The mechanistic implications of this link are unknown at this time, but warrants further study. Our prior work on deletion network analysis of chromatin remodeling complexes led to architectural insights into the complexes (56, 57) which in the case of the SAGA complex was validated by structural biology studies (56). Here our deletion network analysis of the R2TP complex components from the *RVB1-TAP* and *RVB2-TAP* strains have led us in a different direction where changes in protein association found in all deletion strains were also found in gene expression changes in the RNA-Seq analyses. These results demonstrate that deletion network analyses can provide novel and varied insights into cellular systems.

Acknowledgments—The underlying original data not in repositories will be made available in the Stowers Institute Original Data Repository (http://www.stowers.org/research/publications/odr).

* This work was supported by the Stowers Institute for Medical Research.

Ⓢ This article contains supplemental Figs. S1 to S4 and Tables S1 to S9.

** To whom correspondence should be addressed: Stowers Institute for Medical Research, 1000 E. 50th St, Kansas City, MO 64110. Tel.: 816-926-4457; E-mail: mpw@stowers.org.

¶ Current affiliation: DuPont Pioneer, Johnston, Iowa.

‖ Current affiliation: Thermo Fisher Scientific, Waltham, Massachusetts.

REFERENCES

1. Zhao, R., Davey, M., Hsu, Y. C., Kaplanek, P., Tong, A., Parsons, A. B., Krogan, N., Cagney, G., Mai, D., Greenblatt, J., Boone, C., Emili, A., and Houry, W. A. (2005) Navigating the chaperone network: an integrative map of physical and genetic interactions mediated by the hsp90 chaperone. *Cell* **120,** 715–727
2. Te, J., Jia, L., Rogers, J., Miller, A., and Hartson, S. D. (2007) Novel subunits of the mammalian Hsp90 signal transduction chaperone. *J. Proteome Res.* **6,** 1963–1973
3. Boulon, S., Marmier-Gourrier, N., Pradet-Balade, B., Wurth, L., Verheggen, C., Jady, B. E., Rothe, B., Pescia, C., Robert, M. C., Kiss, T., Bardoni, B., Krol, A., Branlant, C., Allmang, C., Bertrand, E., and Charpentier, B. (2008) The Hsp90 chaperone controls the biogenesis of L7Ae RNPs through conserved machinery. *J. Cell Biol.* **180,** 579–595
4. Zhao, R., Kakihara, Y., Gribun, A., Huen, J., Yang, G., Khanna, M., Costanzo, M., Brost, R. L., Boone, C., Hughes, T. R., Yip, C. M., and

Houry, W. A. (2008) Molecular chaperone Hsp90 stabilizes Pih1/Nop17 to maintain R2TP complex activity that regulates snoRNA accumulation. *J. Cell Biol.* **180,** 563–578
5. Boulon, S., Pradet-Balade, B., Verheggen, C., Molle, D., Boireau, S., Georgieva, M., Azzag, K., Robert, M. C., Ahmad, Y., Neel, H., Lamond, A. I., and Bertrand, E. (2010) HSP90 and its R2TP/Prefoldin-like cochaperone are involved in the cytoplasmic assembly of RNA polymerase II. *Mol. Cell* **39,** 912–924
6. Inoue, M., Saeki, M., Egusa, H., Niwa, H., and Kamisaki, Y. (2010) PIH1D1, a subunit of R2TP complex, inhibits doxorubicin-induced apoptosis. *Biochem. Biophys. Res. Commun.* **403,** 340–344
7. Horejsi, Z., Takai, H., Adelman, C. A., Collis, S. J., Flynn, H., Maslen, S., Skehel, J. M., de Lange, T., and Boulton, S. J. (2010) CK2 phospho-dependent binding of R2TP complex to TEL2 is essential for mTOR and SMG1 stability. *Mol. Cell* **39,** 839–850
8. Cloutier, P., Al-Khoury, R., Lavallee-Adam, M., Faubert, D., Jiang, H., Poitras, C., Bouchard, A., Forget, D., Blanchette, M., and Coulombe, B. (2009) High-resolution mapping of the protein interaction network for the human transcription machinery and affinity purification of RNA polymerase II-associated complexes. *Methods* **48,** 381–386
9. Pal, M., Morgan, M., Phelps, S. E., Roe, S. M., Parry-Morris, S., Downs, J. A., Polier, S., Pearl, L. H., and Prodromou, C. (2014) Structural basis for phosphorylation-dependent recruitment of Tel2 to Hsp90 by Pih1. *Structure* **22,** 805–818
10. Gribun, A., Cheung, K. L., Huen, J., Ortega, J., and Houry, W. A. (2008) Yeast Rvb1 and Rvb2 are ATP-dependent DNA helicases that form a heterohexameric complex. *J. Mol. Biol.* **376,** 1320–1333
11. Qiu, X. B., Lin, Y. L., Thome, K. C., Pian, P., Schlegel, B. P., Weremowicz, S., Parvin, J. D., and Dutta, A. (1998) An eukaryotic RuvB-like protein (RUVBL1) essential for growth. *J. Biol. Chem.* **273,** 27786–27793
12. Nano, N., and Houry, W. A. (2013) Chaperone-like activity of the AAA+ proteins Rvb1 and Rvb2 in the assembly of various complexes. *Philos. Trans. R. Soc. Lond. B Biol. Sci.* **368,** 20110399
13. Jonsson, Z. O., Dhar, S. K., Narlikar, G. J., Auty, R., Wagle, N., Pellman, D., Pratt, R. E., Kingston, R., and Dutta, A. (2001) Rvb1p and Rvb2p are essential components of a chromatin remodeling complex that regulates transcription of over 5% of yeast genes. *J. Biol. Chem.* **276,** 16279–16288
14. Jeganathan, A., Leong, V., Zhao, L., Huen, J., Nano, N., Houry, W. A., and Ortega, J. (2015) Yeast Rvb1 and Rvb2 proteins oligomerize as a conformationally variable dodecamer with low frequency. *J. Mol. Biol.* **427,** 1875–1886
15. Tosi, A., Haas, C., Herzog, F., Gilmozzi, A., Berninghausen, O., Ungewickell, C., Gerhold, C. B., Lakomek, K., Aebersold, R., Beckmann, R., and Hopfner, K. P. (2013) Structure and subunit topology of the INO80 chromatin remodeler and its nucleosome complex. *Cell* **154,** 1207–1219
16. Nguyen, V. Q., Ranjan, A., Stengel, F., Wei, D., Aebersold, R., Wu, C., and Leschziner, A. E. (2013) Molecular architecture of the ATP-dependent chromatin-remodeling complex SWR1. *Cell* **154,** 1220–1231
17. Lakomek, K., Stoehr, G., Tosi, A., Schmailzl, M., and Hopfner, K. P. (2015) Structural Basis for Dodecameric Assembly States and Conformational Plasticity of the Full-Length AAA+ ATPases Rvb1.Rvb2. *Structure.* **23,** 483–495
18. Watanabe, S., Tan, D., Lakshminarasimhan, M., Washburn, M. P., Erica Hong, E. J., Walz, T., and Peterson, C. L. (2015) Structural analyses of the chromatin remodelling enzymes INO80-C and SWR-C. *Nat. Commun.* **6,** 7108
19. Lopez-Perrote, A., Munoz-Hernandez, H., Gil, D., and Llorca, O. (2012) Conformational transitions regulate the exposure of a DNA-binding domain in the RuvBL1-RuvBL2 complex. *Nucleic Acids Res.* **40,** 11086–11099
20. Paci, A., Liu, X. H., Huang, H., Lim, A., Houry, W. A., and Zhao, R. (2012) The stability of the small nucleolar ribonucleoprotein (snoRNP) assembly protein Pih1 in Saccharomyces cerevisiae is modulated by its C terminus. *J. Biol. Chem.* **287,** 43205–43214
21. Back, R., Dominguez, C., Rothe, B., Bobo, C., Beaufils, C., Morera, S., Meyer, P., Charpentier, B., Branlant, C., Allain, F. H., and Manival, X. (2013) High-resolution structural analysis shows how Tah1 tethers Hsp90 to the R2TP complex. *Structure* **21,** 1834–1847
22. Mosley, A. L., Sardiu, M. E., Pattenden, S. G., Workman, J. L., Florens, L., and Washburn, M. P. (2011) Highly reproducible label free quantitative proteomic analysis of RNA polymerase complexes. *Mol. Cell. Proteomics* **10,** M110 000687
23. Kim, D., Pertea, G., Trapnell, C., Pimentel, H., Kelley, R., and Salzberg, S. L. (2013) TopHat2: accurate alignment of transcriptomes in the presence of insertions, deletions and gene fusions. *Genome Biol.* **14,** R36
24. Liao, Y., Smyth, G. K., and Shi, W. (2013) The Subread aligner: fast, accurate and scalable read mapping by seed-and-vote. *Nucleic Acids Res.* **41,** e108
25. Love, M. I., Huber, W., and Anders, S. (2014) Moderated estimation of fold change and dispersion for RNA-seq data with DESeq2. *Genome Biol.* **15,** 550
26. Florens, L., and Washburn, M. P. (2006) Proteomic analysis by multidimensional protein identification technology. *Methods Mol. Biol.* **328,** 159–175
27. Banks, C. A., Lee, Z. T., Boanca, G., Lakshminarasimhan, M., Groppe, B. D., Wen, Z., Hattem, G. L., Seidel, C. W., Florens, L., and Washburn, M. P. (2014) Controlling for gene expression changes in transcription factor protein networks. *Mol. Cell. Proteomics* **13,** 1510–1522
28. Zhang, Y., Wen, Z., Washburn, M. P., and Florens, L. (2011) Improving proteomics mass accuracy by dynamic offline lock mass. *Anal. Chem.* **83,** 9344–9351
29. Eng, J. K., McCormack, A. L., and Yates, J. R. (1994) An approach to correlate tandem mass spectral data of peptides with amino acid sequences in a protein database. *J. Am. Soc. Mass Spectrom.* **5,** 976–989
30. Tabb, D. L., McDonald, W. H., and Yates, J. R., 3rd (2002) DTASelect and Contrast: tools for assembling and comparing protein identifications from shotgun proteomics. *J. Proteome Res.* **1,** 21–26
31. Sardiu, M. E., Gilmore, J. M., Groppe, B. D., Herman, D., Ramisetty, S. R., Cai, Y., Jin, J., Conaway, R. C., Conaway, J. W., Florens, L., and Washburn, M. P. (2015) Conserved abundance and topological features in chromatin-remodeling protein interaction networks. *EMBO Rep.* **16,** 116–126
32. Zhang, Y., Wen, Z., Washburn, M. P., and Florens, L. (2010) Refinements to label free proteome quantitation: how to deal with peptides shared by multiple proteins. *Anal. Chem.* **82,** 2272–2281
33. Pavelka, N., Fournier, M. L., Swanson, S. K., Pelizzola, M., Ricciardi-Castagnoli, P., Florens, L., and Washburn, M. P. (2008) Statistical similarities between transcriptomics and quantitative shotgun proteomics data. *Mol. Cell. Proteomics* **7,** 631–644
34. Benjamini, Y., and Hochberg, Y. (1995) Controlling the false discovery rate: A practical and powerful approach to multiple testing. *J. Roy. Statistical Soc.* **57,** 289–300
35. Cherry, J. M., Hong, E. L., Amundsen, C., Balakrishnan, R., Binkley, G., Chan, E. T., Christie, K. R., Costanzo, M. C., Dwight, S. S., Engel, S. R., Fisk, D. G., Hirschman, J. E., Hitz, B. C., Karra, K., Krieger, C. J., Miyasato, S. R., Nash, R. S., Park, J., Skrzypek, M. S., Simison, M., Weng, S., and Wong, E. D. (2012) Saccharomyces Genome Database: the genomics resource of budding yeast. *Nucleic Acids Res.* **40,** D700–D705
36. Kulak, N. A., Pichler, G., Paron, I., Nagaraj, N., and Mann, M. (2014) Minimal, encapsulated proteomic-sample processing applied to copy-number estimation in eukaryotic cells. *Nat. Methods* **11,** 319–324
37. Zhang, W., Zhang, J., Zhang, X., Xu, C., and Tu, X. (2011) Solution structure of the Taf14 YEATS domain and its roles in cell growth of Saccharomyces cerevisiae. *Biochem. J.* **436,** 83–90
38. Florens, L., Carozza, M. J., Swanson, S. K., Fournier, M., Coleman, M. K., Workman, J. L., and Washburn, M. P. (2006) Analyzing chromatin remodeling complexes using shotgun proteomics and normalized spectral abundance factors. *Methods* **40,** 303–311
39. Lee, J. S., Shukla, A., Schneider, J., Swanson, S. K., Washburn, M. P., Florens, L., Bhaumik, S. R., and Shilatifard, A. (2007) Histone crosstalk between H2B monoubiquitination and H3 methylation mediated by COMPASS. *Cell* **131,** 1084–1096
40. Shia, W. J., Osada, S., Florens, L., Swanson, S. K., Washburn, M. P., and Workman, J. L. (2005) Characterization of the yeast trimeric-SAS acetyltransferase complex. *J. Biol. Chem.* **280,** 11987–11994
41. Kakihara, Y., and Houry, W. A. (2012) The R2TP complex: discovery and functions. *Biochim. Biophys. Acta* **1823,** 101–107
42. Kakihara, Y., and Saeki, M. (2014) The R2TP chaperone complex: its involvement in snoRNP assembly and tumorigenesis. *Biomol. Concepts* **5,** 513–520

43. Tanaka, K. (2009) The proteasome: overview of structure and functions. *Proc. Jpn. Acad. Ser.* **85,** 12–36
44. Imai, J., Maruya, M., Yashiroda, H., Yahara, I., and Tanaka, K. (2003) The molecular chaperone Hsp90 plays a role in the assembly and maintenance of the 26S proteasome. *EMBO J.* **22,** 3557–3567
45. Bauer, A., Chauvet, S., Huber, O., Usseglio, F., Rothbächer, U., Aragnol, D., Kemler, R., and Pradel, J. (2000) Pontin52 and Reptin52 function as antagonistic regulators of β-catenin signalling activity. *EMBO J.* **19,** 6121–6130
46. Diop, S. B., Bertaux, K., Vasanthi, D., Sarkeshik, A., Goirand, B., Aragnol, D., Tolwinski, N. S., Cole, M. D., Pradel, J., Yates, J. R., Mishra, R. K., Graba, Y., and Saurin, A. J. (2008) Reptin and Pontin function antagonistically with PcG and TrxG complexes to mediate Hox gene control. *EMBO Rep.* **9,** 260–266
47. Rottbauer, W., Saurin, A. J., Lickert, H., Shen, X., Burns, C. G., Wo, Z. G., Kemler, R., Kingston, R., Wu, C., and Fishman, M. (2002) Reptin and Pontin Antagonistically Regulate Heart Growth in Zebrafish Embryos. *Cell* **111,** 661–672
48. Kim, J. H., Kim, B., Cai, L., Choi, H. J., Ohgi, K. A., Tran, C., Chen, C., Chung, C. H., Huber, O., Rose, D. W., Sawyers, C. L., Rosenfeld, M. G., and Baek, S. H. (2005) Transcriptional regulation of a metastasis suppressor gene by Tip60 and beta-catenin complexes. *Nature* **434,** 921–926
49. Makino, Y., Kanemaki, M., Kurokawa, Y., Koji, T., and Tamura, T.-a. (1999) A Rat RuvB-like Protein, TIP49a, Is a Germ Cell-enriched Novel DNA Helicase. *J. Biol. Chem.* **274,** 15329–15335
50. Kanemaki, M., Kurokawa, Y., Matsu-ura, T., Makino, Y., Masani, A., Okazaki, K., Morishita, T., and Tamura, T. A. (1999) TIP49b, a New RuvB-like DNA Helicase, Is Included in a Complex Together with Another RuvB-like DNA Helicase, TIP49a. *J. Biol. Chem.* **274,** 22437–22444
51. Mbantenkhu, M., Wang, X., Nardozzi, J. D., Wilkens, S., Hoffman, E., Patel, A., Cosgrove, M. S., and Chen, X. J. (2011) Mgm101 is a Rad52-related protein required for mitochondrial DNA recombination. *J. Biol. Chem.* **286,** 42360–42370
52. Rice, D. W., Rafferty, J. B., Artymiuk, P. J., and Lloyd, R. G. (1997) Insights into the mechanisms of homologous recombination from the structure of RuvA. *Curr. Opin. Struct. Biol.* **7,** 798–803
53. Morrison, A. J., and Shen, X. (2009) Chromatin remodelling beyond transcription: the INO80 and SWR1 complexes. *Nat. Rev. Mol. Cell Biol.* **10,** 373–384
54. Moller, A., Xie, S. Q., Hosp, F., Lang, B., Phatnani, H. P., James, S., Ramirez, F., Collin, G. B., Naggert, J. K., Babu, M. M., Greenleaf, A. L., Selbach, M., and Pombo, A. (2012) Proteomic analysis of mitotic RNA polymerase II reveals novel interactors and association with proteins dysfunctional in disease. *Mol. Cell. Proteomics* **11,** M111 011767
55. Gnatovskiy, L., Mita, P., and Levy, D. E. (2013) The human RVB complex is required for efficient transcription of type I interferon-stimulated genes. *Mol. Cell. Biol.* **33,** 3817–3825
56. Lee, K. K., Sardiu, M. E., Swanson, S. K., Gilmore, J. M., Torok, M., Grant, P. A., Florens, L., Workman, J. L., and Washburn, M. P. (2011) Combinatorial depletion analysis to assemble the network architecture of the SAGA and ADA chromatin remodeling complexes. *Mol. Syst. Biol.* **7,** 503
57. Sardiu, M. E., Gilmore, J. M., Carrozza, M. J., Li, B., Workman, J. L., Florens, L., and Washburn, M. P. (2009) Determining protein complex connectivity using a probabilistic deletion network derived from quantitative proteomics. *PloS one* **4,** e7310